applied mechanics

Article

Comparison of the Biomechanical Behavior of a Soft Bankart Lesion on Shoulder Ligaments During Abduction: A Finite Element Study

Maria de la Luz Suarez-Hernandez [1,*], Guillermo Urriolagoitia-Sosa [1,*], Beatriz Romero-Ángeles [1,*], Francisco Javier Gallegos-Funes [1], Francisco Carrasco-Hernández [2], Edder Jair Rodríguez-Granados [1], Gabriela Ramirez-Sanchez [1], Jonathan Rodolfo Guereca-Ibarra [1], Jorge Alberto Gomez-Niebla [1] and Jonatan Mireles-Hernández [1]

[1] Instituto Politécnico Nacional, Escuela Superior de Ingeniería Mecánica y Eléctrica, Sección de Estudios de Posgrado e Investigación Edificio 5, 2do. Piso, Col. Lindavista, Alc. Gustavo A. Madero, Ciudad de México 07320, Mexico; fgallegosf@ipn.mx (F.J.G.-F.); erodriguezg2005@alumno.ipn.mx (E.J.R.-G.); gramirezs2500@alumno.ipn.mx (G.R.-S.); jguerecai2200@alumno.ipn.mx (J.R.G.-I.); jgomezn2200@alumno.ipn.mx (J.A.G.-N.); jmirelesh@ipn.mx (J.M.-H.)

[2] Departamento Académico de Mecatrónica y Energías Renovables, Universidad Tecnológica de Durango, Carretera Durango-Mezquital, km 4.5 Gabino Santillán, Durango 34308, Mexico; francisco.carrasco@utd.edu.mx

* Correspondence: luzsuarez398@gmail.com (M.d.l.L.S.-H.); guiurri@hotmail.com (G.U.-S.); bromeroa@ipn.mx (B.R.-Á.)

Abstract

The soft Bankart lesion is characterized by the abnormal translation of the humeral head during dislocation, which places excessive stress on the labrum and causes it to stretch along with other structures that provide joint stability. This lesion is described as a purely soft tissue injury and occurs due to the detachment of the anteroinferior labroligamentous complex. This research aimed to evaluate the computational biomechanics of a biomodel of the shoulder joint with a soft Bankart lesion during pure abduction using the Finite Element Method (FEM). It evaluates the tissue mechanics of the structures with the lesion, such as ligaments, the articular capsule, and the labrum, which guide and limit the bones of the joint during movement. A healthy shoulder joint biomodel is developed for comparison. The results of stress and strain in the healthy shoulder and the soft Bankart biomodel are analyzed. The results for the soft Bankart biomodel show an increase in stress on the MGHL, with the pIGHL assuming a primary stabilizing role. The CHL and articular capsule limit the excessive displacement of the humeral head.

Keywords: FEM analysis; soft Bankart lesion; shoulder biomodel; tissue mechanics; computational biomechanics; FEM

Check for updates

Received: 26 May 2026
Revised: 10 July 2026
Accepted: 19 July 2026
Published: 27 July 2026

1. Introduction

The shoulder joint has a high rate of dislocations in the human body due to its morphological instability: a shallow glenoid cavity that articulates with the humeral head, which has an almost spherical geometry [1]. This configuration allows for a wide range of motion. To maintain joint congruency, the joint is stabilized by a complex system of dynamic stabilizers (muscles) and static stabilizers (ligaments, labrum, cartilage and joint capsule). Ligaments function as passive restraints that guide and control movement at low loads by directing the movement within a safe range; at high loads, they serve to resist and limit excessive movement [2].

This wide range of motion makes the shoulder joint prone to a variety of injuries. Young adults often experience anterior shoulder dislocation, presenting a soft Bankart lesion. This occurs due to the abnormal translation of the humeral head during dislocation, which places excessive stress on the labrum and causes it to stretch along with other structures that provide joint stability [3,4]. Sports such as rugby, American football, basketball, and tennis are high-risk activities for developing a soft Bankart lesion, particularly with sudden or repetitive overhead movements [5,6]. The soft Bankart lesion is located between 3 and 6 o'clock in the glenoid cavity, which distinguishes it from other labrum tears, such as the SLAP lesion [7]. This lesion is described as a purely soft tissue injury (defined as a tear in the articular capsule, labrum, and ligament), without any bony defect presented in the humeral head, as shows in Figure 1. The lesion occurs due to the detachment of the anteroinferior labroligamentous complex, which tears away from the glenoid cavity. At the same time, the joint capsule and the inferior glenohumeral ligament (aIGHL) present a tear [8].

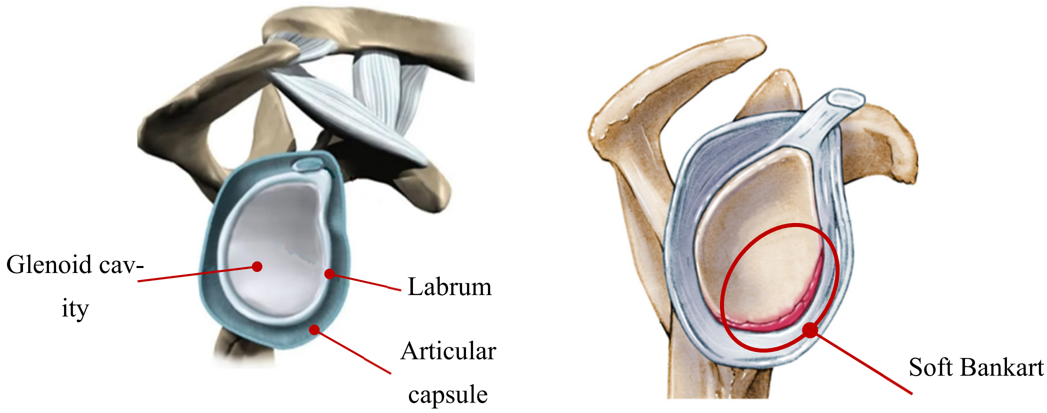

Figure 1. Glenoid cavity in the sagittal plane. (**Left**): healthy joint; (**right**): Soft Bankart lesion.

In recent years, biomechanical research focused on the glenohumeral joint has progressed significantly due to the development of finite element models based on three-dimensional representations. With reference to the soft tissues of the joint, studies have evaluated the behavior of SLAP tears [9–12] in the superior labrum and articular capsule. In addition, a numerical analysis of humeral head displacement resulting from bony defects associated with anterior shoulder instability has been conducted [13,14]. Previous investigations have focused on the remplissage procedure [14–16]. However, despite these advances, there remains a significant gap in the specific numerical evaluation of the soft Bankart lesion, which is a capsulolabral tear without a significant bony component. This lack of a finite element biomodel explicitly focused on the soft Bankart limits the understanding of the mechanisms underlying the variety of lesions that affect the internal behavior and interaction of the glenohumeral joint tissues. This justifies the development of a controlled simulation that allows for the integral quantification of stress redistribution across the glenohumeral ligaments and articular capsule. Additionally, the simulation of pure abduction movement under controlled loading conditions (using only the force of the supraspinatus) isolates the passive mechanical effect of the Bankart tear on the connecting tissues, eliminating the effect of the compensatory muscle forces that would otherwise interfere with the results.

In biomedical engineering, a biomodel often refers to a three-dimensional model characterized by its ability to virtually replicate biological systems [17,18]. This study aims to develop a three-dimensional model of the shoulder joint, both healthy and with a soft

Bankart lesion, to conduct a numerical analysis capable of quantifying and comparing changes in ligament stress and strain, directly contrasting the results between the healthy joint and the soft Bankart lesion.

2. Materials and Methods

A finite element analysis was conducted on both biomodels of a healthy shoulder joint and a soft Bankart lesion to compare the biomechanical soft tissue responses of the shoulder during pure abduction. The biomodel includes the humerus, scapula, and clavicle bones (each with cortical and cancellous components), as well as the articular capsule, labrum, and ligaments. This allows for a detailed examination of the behavior and interaction between soft tissues during movement. A discretization convergence analysis was performed to assess the accuracy and efficiency of the numerical model. This investigation aims to evaluate stress distribution numerically by comparing ligament stress between biomodels [9,19,20].

2.1. Modeling of the Computational Shoulder Joint

Computational modeling corresponds to a three-dimensional representation of different biological structures within the human body. By utilizing medical imaging and CAD software tools 2025, it is feasible to develop virtual anatomical structures [21–23]. The process begins with CT images of a 23-year-old female volunteer's torso; the images contained within the DICOM file offer detailed insights into the spatial dimensions and anatomical positions of internal body structures. The images in DICOM format were imported into Mimics Research (version 21.0) software to delineate and define the contours of the structures that are part of the biomodel. For cortical and cancellous bone, a combination of automatic thresholding and manual segmentation masks was applied. Anatomical references documented in previous publications were used as guides for the origin and insertion of the capsule and ligaments [24,25]. Figure 2 shows the tissue mask of the shoulder joint.

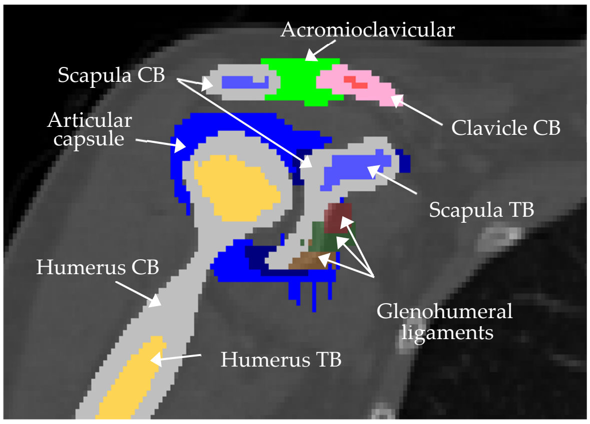

Figure 2. Coronal view of manual segmentation masks of the model using Mimics Research (version 21.0).

The articular capsule was reconstructed according to the measurements from the CT images in the volunteer's data. A 4 mm thickness is included at the end of the capsule and the scapular bone to represent the labrum [26]. The articular capsule was divided into five regions. Their limits were determined based on the quadrants of the glenohumeral joint (posterosuperior, anterosuperior, anteroinferior and posteroinferior) [27]; the axillary recess was included.

The next step is structure refinement, which consists of improving the elements' surfaces, removing duplicated surfaces, repairing cavities or other issues, and smoothing the geometry [9]. Boolean operations were used to cut between the geometric structures to ensure consistency between them. To accurately simulate a soft Bankart lesion, the model was refined by removing elements corresponding to the MGHL and the articular capsule geometry, representing the detachment of the anteroinferior capsulolabral glenoid. This approach ensures that the resulting biomodel closely replicates the anatomical alterations described in clinical cases of soft Bankart lesions [7,8,28]. Once the refinement process and modifications are complete, the volumes of both models (healthy shoulder and shoulder with a soft Bankart lesion) are generated for further analysis. Each element for the biomodels is saved in STL format. This process was conducted using Materialise 3-matic (version 13.0) software.

Both the healthy shoulder joint biomodel and the biomodel with a soft Bankart lesion were developed and analyzed using finite element analysis software, like ANSYS Workbench (version 2021 R2; ANSYS Inc. Canonsburg, PA, USA). For the numerical simulations, certain parameters were established, including model discretization, assignment of mechanical properties to the biological structures, definition of boundary conditions, and remote forces, providing a comprehensive and reliable biomechanical evaluation of both models. Figure 3 summarizes the steps for the development of the shoulder biomodel.

2.2. Biomodel Discretization

To assess the quality of the tetrahedral mesh for the ligament structures included in the models, they were evaluated using the skewness metric implemented in ANSYS. For tetrahedral elements, ANSYS calculates a volumetric skewness based on the formula for the ideal volume of a regular tetrahedron as a function of the radius of a circle [29,30]. The ideal volume of a regular tetrahedron is obtained using Equation (1):

$$V_{ideal} = \frac{8\sqrt{3}}{27}R^3 \tag{1}$$

Skewness is then defined as

$$\text{skewness} = 1 - \frac{V}{V_{ideal}} \tag{2}$$

where V is the actual volume of the tetrahedron. A skewness value close to 0 indicates a nearly regular element, while values close to 1 indicate significant distortion or volume collapse [31]. Additionally, ANSYS reports an angular skewness defined as

$$\text{skewness}_{angle} = \left(\frac{\theta_{max} - \theta_e}{180^\circ - \theta_e}, \frac{\theta_e - \theta_{min}}{\theta_e}\right) \tag{3}$$

where θ_{max} and θ_{min} are, respectively, θ_e the maximum and minimum internal angles, and is the ideal angle corresponding to the equilateral shape of the face. The final skewness reported by ANSYS is the maximum volumetric and angular skewness [32]. Three different mesh densities with element sizes of 1.5 mm, 1 mm and 0.8 mm were generated in the healthy model. A torque of 10 N was applied to the distal humerus for abduction. The mesh was considered convergent if the differences in results were within a 5% accuracy margin for the coarse and fine meshes [33]. For each mesh configuration, the maximum stress in the ligaments was calculated. The coarse and medium meshes presented a variation of 15% in the maximum stress value. But the difference between the medium mesh and the smaller mesh exhibited a difference of around 4%.in the articular capsule stress. The mesh of 1 mm of solid tetrahedral elements effectively captured the complex morphology of the ligaments and was based on previous studies of convergence in glenohumeral joints [34]. The articular capsule regions were meshed individually with quadrilateral shell elements of 1 mm [35,36].

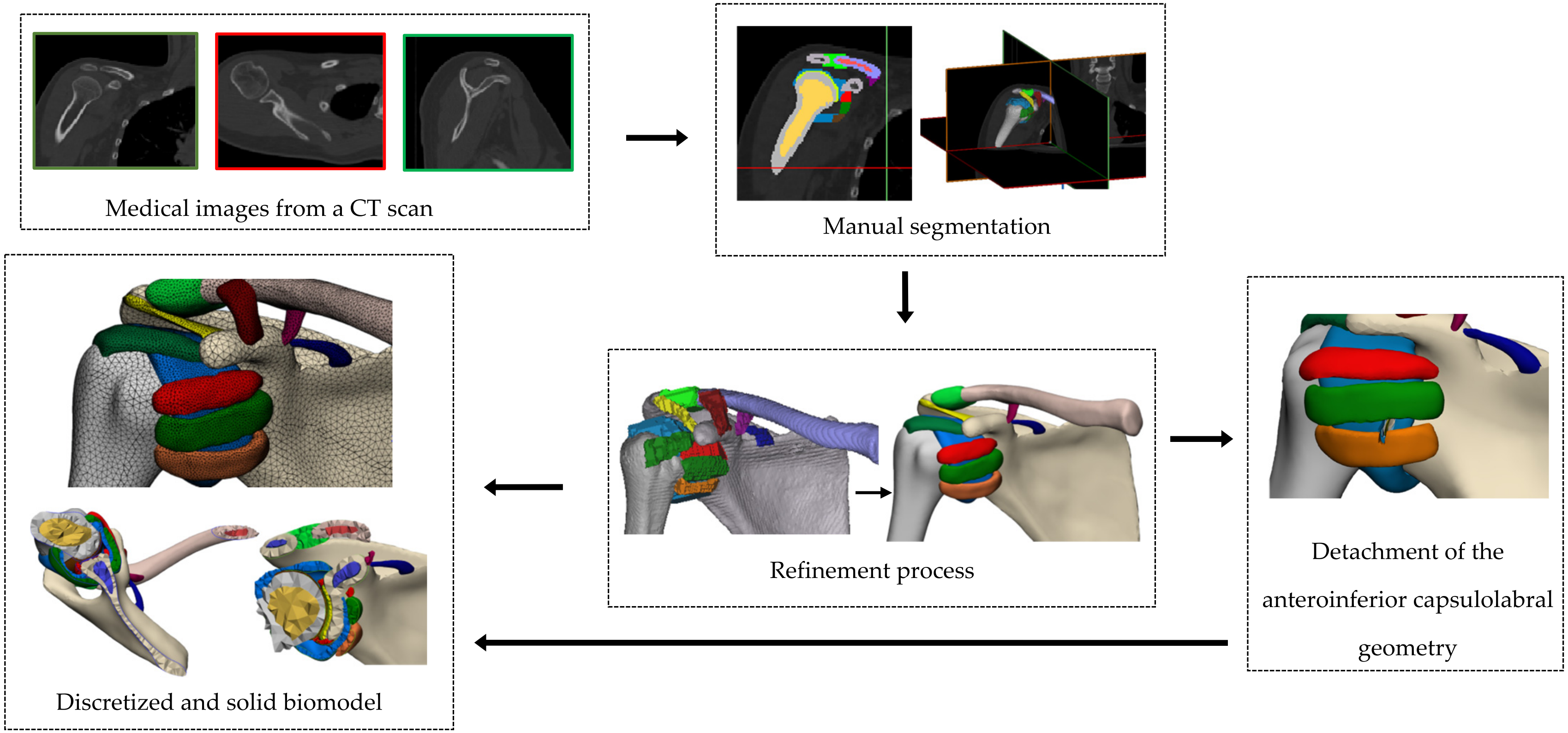

Figure 3. Schematic development of the shoulder joint biomodel in Materialise 3-matic v13.0.

Figure 4 shows the skewness quality mesh metric. It is considered very good. It presents an average of 0.32508 for the healthy shoulder biomodel and 0.32891 for the soft Bankart lesion. This ensures the avoidance of numerical errors and model convergence, following standard recommendations for meshing. Table 1 shows the comparison of nodes and elements of the modified structures to represent the lesion.

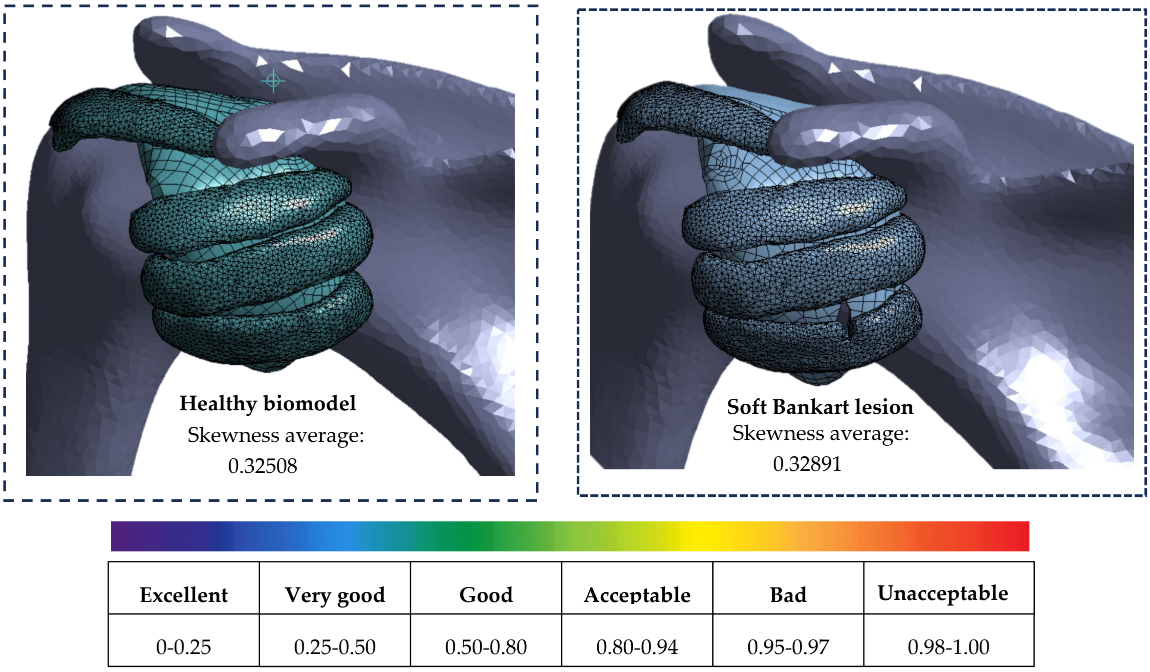

Figure 4. Average skewness for the biological structures that are affected by the soft Bankart.

Table 1. Comparison of elements and nodes between the structures modified to represent the soft Bankart lesion and the healthy biomodel.

Biological Tissue	Healthy Biomodel		Soft Bankart Lesion	
	Nodes	Elements	Nodes	Elements
aIGHL	15,787	9433	17,800	10,532
Articular capsule and labrum	1551	1478	1515	1406

Table A1 provides a list of nodes and elements corresponding to the structures representing the soft tissues in both biomodels, healthy shoulder and the soft Bankart lesion.

2.3. Boundary Conditions and Loading

Contact regions are defined to represent ligament insertions into the bone; the contact type is set to boned. For contacts between the ligaments and the joint capsule, a frictionless contact was defined, allowing free sliding between tissues [9,37].

A local coordinate system was defined [38] on the humeral head, the distal edge of the scapula, and the acromion end of the clavicle (where movements and rotations are restricted during simulations based on published results from previous research) [38–41]. Figure 5 shows the boundary and load condition established.

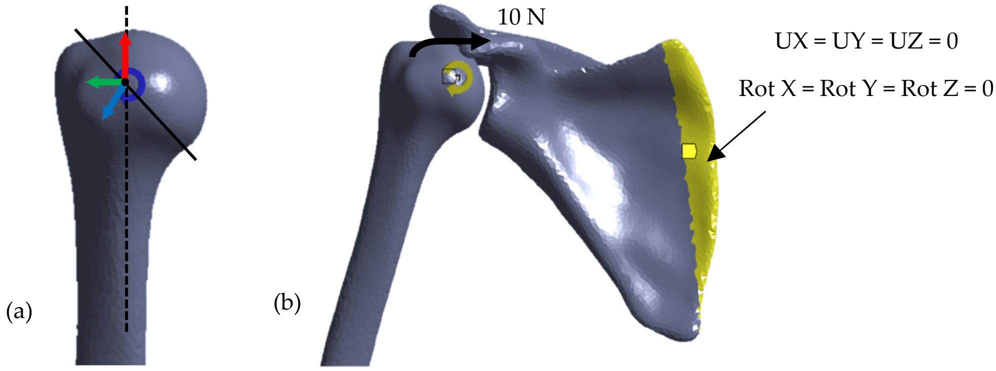

Figure 5. Boundary conditions for the finite element: (**a**) Local coordinate system at the center of the humeral head. (**b**) 10 N force applied in the supraspinatus tendon area and revolute joint (yellow arrow) in the humerus for abduction; distal edge of the scapula fixed (scapula yellow area).

2.4. Mechanical Properties of Biomodel Biological Structures

In the numerical modeling of soft tissues using the finite element method, the choice of a hyperelastic constitutive model is critical for accurately reproducing the stress and strain fields under different loading conditions. Among the various formulations, the Mooney–Rivlin model is favored for its balance between mathematical simplicity and the ability to describe the nonlinear behavior of nearly incompressible materials. The model is based on a strain-energy density function [42]. The deformation energy density function W for an incompressible, isotropic material is usually expressed as:

$$W = C_{10}(I_1 - 3) + C_{01}(I_2 - 3) \tag{4}$$

where I_1 and I_2 are the first and second invariants of the Cauchy–Green deformation tensor, and C_{10} and C_{01} are Mooney–Rivlin material parameters. To model the near-incompressibility characteristics of soft tissues, a volumetric term is included. This is commonly implemented in finite element software like Ansys. The equation adding the volumetric term would be expressed as:

$$W = C_{10}(I_1 - 3) + C_{01}(I_2 - 3) + \frac{1}{D_1}(J - 1)^2 \tag{5}$$

where D_1 is the incompressible parameter, which is inversely proportional to the volumetric compressibility modulus [43]. The mechanical properties of the bones, labrum, articular capsule and ligaments were adapted from previous studies based on experimental data from mechanical tests on human cadaveric tissue, summarized in Table 2 [37,44–47]. To represent nonlinear material behavior, the Mooney–Rivlin model is applied with parameters adopted from the literature for soft tissues, as specified in Table 2. The humerus, clavicle, and scapula are assumed to be rigid body material due to their high stiffness compared to soft tissues [48].

Biological tissues present variability in their mechanical properties due to age, pathology, or experimental uncertainty. Therefore, a local sensitivity analysis was performed in the articular capsule by varying Young's modulus over a range of 10%, 20% and 30% to quantify how uncertainty in material stiffness affects the maximum stress.

https://doi.org/10.3390/applmech7030061

Table 2. Mechanical properties of soft tissues.

Structure	Type	Mechanical Properties	Reference
Humerus	Rigid body	E = 15,000 MPa, v = 0.3	[44,48]
Scapula			[44,48]
Clavicle			[44,48]
Labrum	Mooney–Rivlin model	$C_{10} = 2.8$ $C_{01} = 2.8$ $D_1 = 0.004$	[45]
Articular capsule		$C_{10} = 6$ $C_{01} = 6.5$ $D_1 = 0.12$	[47]
Glenohumeral ligaments		$C_{10} = 14.4$ $C_{01} = 14.4$ $D_1 = 0.008$	[46]

3. Results

The results below demonstrate the role of static stabilizers in the joint, directly comparing ligament stress during humeral motion in both healthy conditions and in the presence of a Bankart soft-tissue lesion. Figure 6 shows stress results indicating that most ligaments exhibit an increase in stress values in the shoulder with the lesion. Positive stress indicates that the ligament is actively resisting the load and acts as a restricting force, preventing excessive displacement of the humeral head. Negative stress represents compression, indicating that the structure is folding or bunching. The CHL is a band that connects the coracoid to the humerus, and as the humerus rises, the ligament shortens during abduction [25]. The previous statement is consistent with the negative stress value obtained: -0.05485 MPa for the healthy shoulder compared to -0.08867 MPa for the soft Bankart. The negative values represent the compression of the ligament while the arm rises in abduction. This behavior is also observed in the SGHL, which shows 67% more compression compared to the same ligament in the healthy shoulder. The pGHL of the shoulder with the lesion presents an increase of 57% with respect to the healthy ligament. The rest of the glenohumeral ligaments show a slight increase in stress in the structures of the biomodel with the lesion.

Figure 7 shows significant changes in the stress distribution in zones of the articular capsule. The anteroinferior and posteroinferior regions of the capsule present a marked increase, with values of 0.34248 MPa compared to 0.11981 in the healthy anteroinferior region. The posteroinferior region of the articular capsule with the lesion presents an increase of 67%. The area of the axillary recess of the healthy biomodel shows negative stress, indicating tissue compression and damping of the humeral head's movement, but the biomodel with the lesion presents a marked increase, with values of 0.5779 MPa compared to -0.125 MPa.

Visual Results for the Numerical Analysis

The visual results from the numerical analysis in the ANSYS Workbench (version 2021 R2; ANSYS Inc. Canonsburg, PA, USA) software show stress distribution (Figure 8). The maximum stress values are associated with the glenohumeral ligaments and the humerus. In the healthy biomodel, stress distribution occurs among the CHL, articular capsule, and glenohumeral ligaments. Conversely, the pathological biomodel shows areas of concentrated stress: CHL, labrum, and pIGHL, which work together to maintain joint congruency, avoiding excessive displacement of the humeral head.

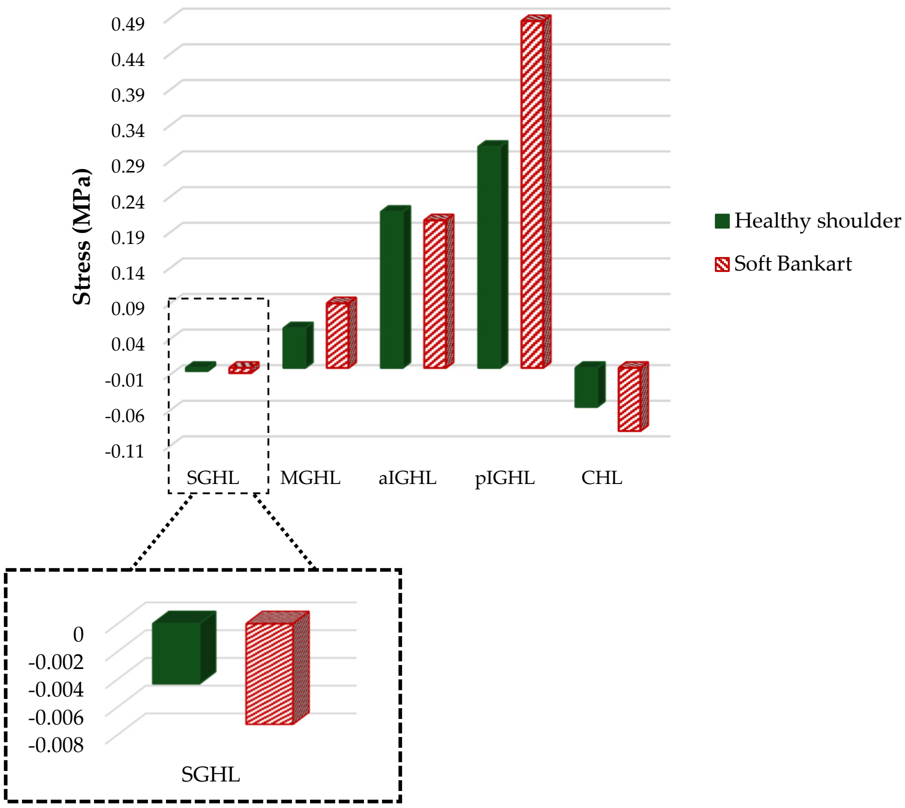

Figure 6. Stress results for the structures connecting the arm to the torso.

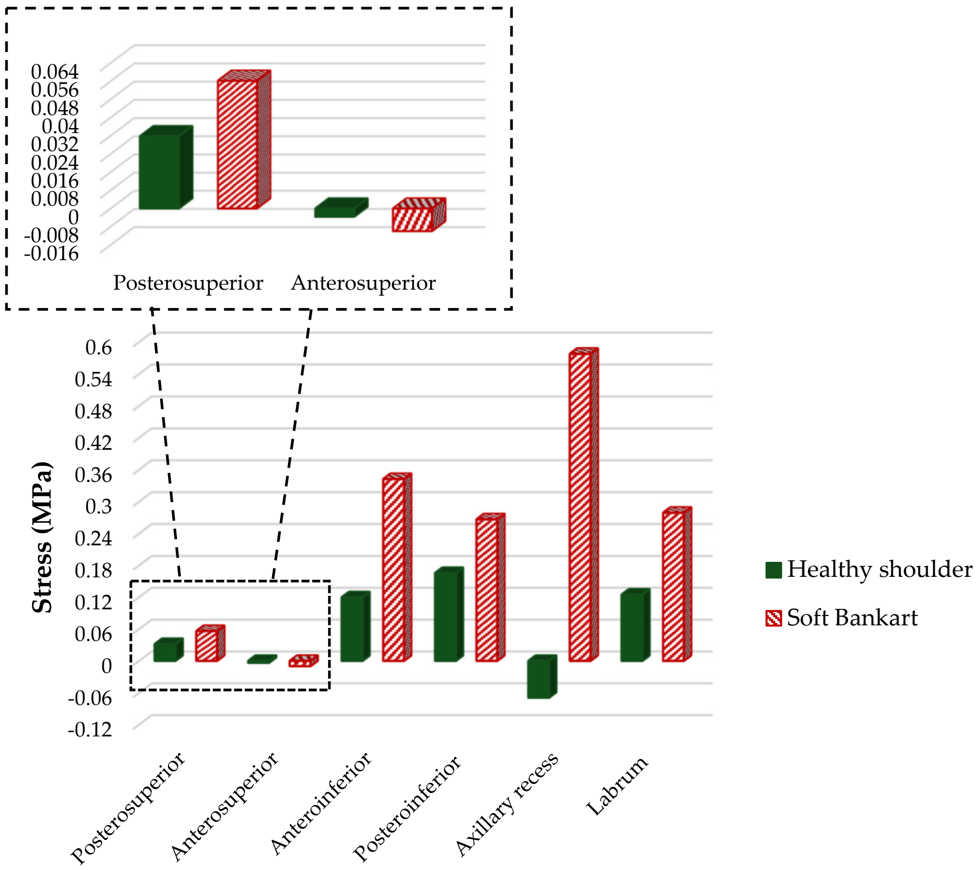

Figure 7. Stress results for the articular capsule, axillary recess, and labrum.

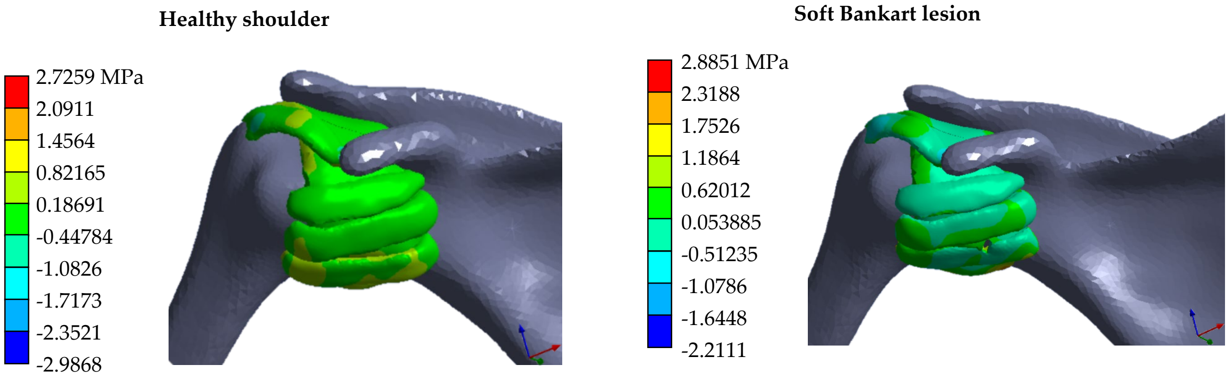

Figure 8. Stress visual results from ANSYS Workbench.

Figure 9 shows tissue strain as the arm is raised. The left column shows the results for the healthy shoulder. The column on the right shows the visual results of the biomodel representing soft Bankart tissue injury. In the healthy biomodel, the pGHL shows a maximum value of 16% compression at the junction with the scapula. The axillary recess also presents a maximum value of 16%. The CHL presents values of 3.5% in the soft Bankart model and 2.7% in the healthy model. The posteroinferior area of the labrum presents a compression value of 16%. In the articular capsule with soft Bankart, the posteroinferior region shows a maximum value of 3%, while the anteroinferior region presents a compression value of −7%. The same articular capsule regions present values of 1.9% and a compression value of 5%, interpreted as capsular laxity, which alters the glenohumeral joint stability. Stress distribution is not uniform in the model with the Bankart lesion, resulting in a 21% difference compared with the healthy joint, indicating an abnormal redistribution of compression load between the structures that could compromise joint stability and increase the risk of recurrent dislocation.

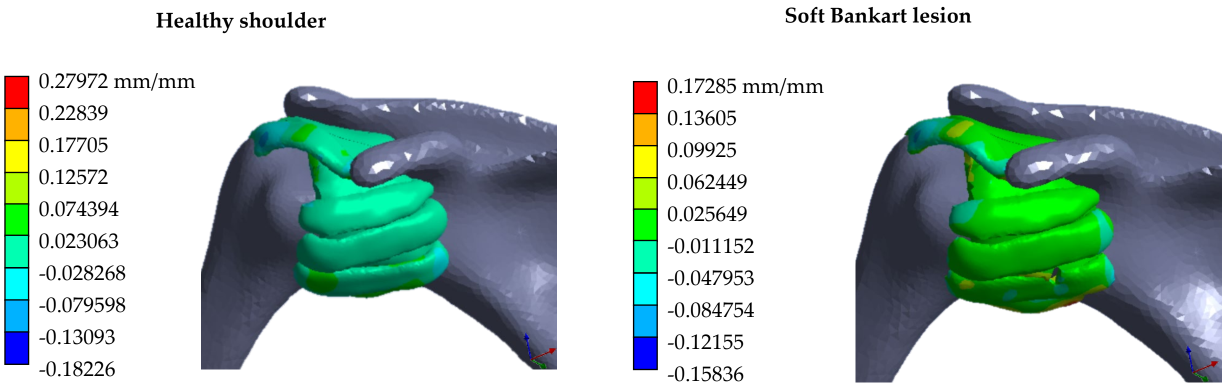

Figure 9. Strain visual results from ANSYS Workbench.

A parametric sensitivity analysis was performed by varying the Young's modulus of the articular capsule by ±10%, ±20% and ±30% increases. For each variation, the maximum stress was calculated using the shoulder finite element model under replicated load conditions. The standard derivation of the maximum stress was calculated as 0.572 MPa, indicating a variability of approximately ±0.572 MPa around the mean value.

4. Discussion

The finite element numerical simulation results provide relevant information about the behavior of the static stabilizers in shoulder structures during pure abduction with a soft Bankart lesion. The comparative analysis between the healthy biomodel and the injured biomodel reveals significant alterations in joint behavior, including changes in the distribution of stress and strain within structures such as ligaments, the joint capsule, and the labrum, providing a deeper understanding of the pathophysiology of anterior glenohumeral instability. One of the most significant findings of this analysis is the presence of negative tension values in the CHL and SHL ligaments during movement, indicative of physiological laxity. During pure abduction, as the humerus elevates, the CHL shortens due to a reduction in the distance between its insertion points, leading to ligament contraction [25]. These observations align with the negative stress results and reflect contraction rather than elongation. The MGHL tightens by 37% compared to the healthy side, acting as a barrier against the anterior displacement of the humeral head. This finding could explain the progression of capsular lesions observed in cases of chronic recurrent instability [49]. The pGHL becomes the main static stabilizer, exceeding the stress of the MGHL, which has a lower value [50]. The labrum improves shoulder stability by increasing the depth and surface area of the joint, centering the humeral head. It also acts as a joint seal to maintain intra-articular pressure [51]. This is reflected in the analysis results, which show negative stress values indicating the damping effect of the humeral head's movement. This indicates that the affected labrum does not contain or center the humeral head; therefore, the anteroinferior and posteroinferior regions of the capsule, as well as the axillary recess, play a role in holding the humeral head in position. The visual results of the biomodel with a soft Bankart lesion show a reduction in movement damping; however, areas where the humeral head's cushioning is concentrated are highlighted. This is consistent with the onset of degenerative changes and glenohumeral osteoarthritis [52,53]. An increase in stress is observed in the axillary recess, with maximum values of 0.5779 MPa during pure abduction. This increase is probably due to a phenomenon of inferior capsular tension caused by excessive translation of the humeral head. Despite the results, the study presents several limitations. Among them is the assumption that the biomodel's structures were made of isotropic materials. The articular capsule and the labrum have complex collagen fiber architectures that can give rise to anisotropic and region-dependent mechanical behavior. The simplifications made in this study neglect the directional dependence of the mechanical response and may lead to inaccuracies in stress distribution and strain localization. The data are from physical tests performed on elderly cadaver shoulder joints, which may not fully represent in vivo conditions due to tissue degeneration, age variability, and the absence of muscle activation. Due to this, the mechanical response may differ from that of a living human with a soft Bankart tear in the glenohumeral joint, even though relative trends between simulated joint movements are expected to remain informative. Another important limitation is that the definition of the enthesis (attachment) of ligaments in bones is based on a combination of anatomical references from the literature and manual selection based on segmented geometry, which introduces potential variability. Future studies should use automatic recording techniques or soft-tissue-resolution magnetic resonance imaging to define the enthesis more precisely and specifically for each patient. One more fundamental limitation of the model presented here is that it controls the force exerted purely by the supraspinatus muscle, which plays a leading role during the early stages of arm abduction [54]. In subsequent biomodels, it would be appropriate to apply the forces representing the deltoid, infraspinatus, and teres minor muscles to assess how the compensation of the anterior support influences stress redistribution in the joint's soft tissues. In addition, the model's information is collected from a single subject performing a pure abduction movement without external rotation of the humerus, so morphological differences between individuals and differences in movement may result in variations in stress distribution. Furthermore, the finite element numerical simulation does not fully represent the internal functioning of the human body joint.

5. Conclusions

The results show that during a soft Bankart lesion, in pure abduction, the CHL and articular capsule limit excessive displacement of the humeral head during movement. An increase in stress on the pIGHL ligament was observed, assuming a primary stabilizing role and effectively restricting excessive translation of the humeral head during abduction. Building on these biomechanical insights and advances in technology, it is possible to develop numerical simulations of bone geometries using finite elements, following an increasingly standardized methodology that generally involves reconstructing bone geometry from medical images, assigning mechanical properties derived from bone mineral density, and defining load conditions. In contrast, soft tissues (ligaments and joint capsule) are sensitive to local physiological conditions and exhibit non-linear mechanical responses. This inconsistency between the maturity of bone models and the challenge of representing soft tissue underscores the need to continue developing strategies to simulate tissue behavior under loads that better reflect reality. In numerical simulations, ligaments and capsules are simplified in their geometry and structure, represented by elements such as rectangular bands, springs, or connecting lines, due to the difficulty of obtaining detailed geometry and in vivo experimental data on stiffness and damage. Despite these limitations, image-based numerical models have the potential to transform surgical planning and rehabilitation in orthopedics. Patient-specific models enable the prediction of changes in joint tissues in a virtual environment. This capability can help the surgeon select the most appropriate technique and reduce the risk of mechanical complications. It should be emphasized that, although biomodels based on medical images facilitate visualization of the specific patient's joint and help interpret the distribution of forces, contact pressures, and range of motion, they do not replace clinical experience. This contrast underlines that clinical expertise remains essential even with advanced modeling tools. The advancement and implementation of these models are completely linked to the expertise of mechanical engineers and medical specialists. Methodologically, these professionals make critical contributions to mechanics, constitutive model formulation, finite element analysis, and experimental validation—elements that are fundamental to transforming medical images into computational representations of the musculoskeletal system. Moreover, mechanical engineers play a pivotal role in the design of implants, fixation devices, and simulation platforms, all of which benefit directly from the insights these models provide. Through their involvement, they bridge the gap between mechanical understanding and technological innovation within the field of orthopedics. In summary, reflecting this collaborative and technological evolution, this study describes the broader trend toward the use of patient-specific biomechanical models generated from medical images as tools to aid in diagnosis, surgical planning, and rehabilitation of the shoulder and other complex joints. Continued progress in this field stands to enhance patient care and set new standards in orthopedic practice. While modeling bones is relatively straightforward, accurately representing soft tissues remains a significant challenge. This contrast highlights the necessity of ongoing advancements in image acquisition, segmentation, material characterization, and experimental validation techniques.

Author Contributions: Conceptualization, M.d.l.L.S.-H., G.U.-S. and F.J.G.-F.; methodology, M.d.l.L.S.-H. and J.A.G.-N.; software, M.d.l.L.S.-H., B.R.-Á. and J.M.-H.; validation, M.d.l.L.S.-H. and E.J.R.-G.; formal analysis, M.d.l.L.S.-H.; investigation, F.J.G.-F. and F.C.-H.; resources, M.d.l.L.S.-H. and J.A.G.-N.; data curation, G.U.-S. and G.R.-S.; writing—original draft preparation, B.R.-Á. and E.J.R.-G.; writing—review and editing, F.J.G.-F. and G.R.-S.; visualization, M.d.l.L.S.-H. and J.R.G.-I.; supervision, G.U.-S. and F.C.-H.; project administration, G.U.-S. and B.R.-Á. All authors have read and agreed to the published version of the manuscript.

Funding: This research received no external funding.

Institutional Review Board Statement: Not applicable.

Informed Consent Statement: Not applicable.

Data Availability Statement: The CT dataset contains identifiable human data and is not publicly available due to privacy restrictions. De-identified data derived are available from the corresponding author upon reasonable request. No third-part data were used.

Acknowledgments: The authors gratefully acknowledge the Instituto Politécnico Nacional and the Secretaría de Ciencias, Humanidades, Tecnología e Innovación (SECIHTI) for the support provided for this research.

Conflicts of Interest: The authors declare no conflicts of interest.

Abbreviations

The following abbreviations are used in this manuscript:

SGHL	Superior glenohumerla ligament
MGHL	Medial glenohumeral ligament
aIGHL	Anterior band of the inferior glenohumeral ligament
pIGHL	Posterior band of the inferior glenohumeral ligament
CHL	Coracohumeral ligament

Appendix A

Table A1 shows the elements and nodes of the structures that were not modified to replicate the soft Bankart lesion, representing the solid tetrahedral soft tissues of both biomodels of the shoulder joint.

Table A1. Elements and nodes of the solid structures of the biomodel.

Biological Tissue	Nodes	Elements
SGHL	11,453	6610
MGHL	17,016	10,106
pIGHL	11,605	6635
CHL	11,212	6403

References

1. Chang, L.R.; Anand, P.; Varacallo, M.A. Anatomy, shoulder and upper limb, glenohumeral joint. In *StatPearls*; StatPearls Publishing: Treasure Island, FL, USA, 2025.
2. Panjaitan, T. Anatomy and Biomechanic of the Shoulder. *Orthop. J. Sports Med.* **2019**, *7*, 2325967119S00466. [CrossRef]
3. Aryana, I.G.N.W.; Febyan, F.; Prabawa, M.N.A. Bankart lesion cases with bone or soft tissue procedure as various methods available; A systematic review. *Int. J. Med. Rev.* **2025**, *12*, 864–871. [CrossRef]
4. Grewal, R.S.; Berger, G.K.; Pennock, A.T.; Bomar, J.D.; Edmonds, E.W. Outcomes of arthroscopic bony Bankart repair compared with soft-tissue only Bankart repair in the adolescent population. *J. Pediatr. Orthop.* **2026**, *ahead of print*. [CrossRef] [PubMed]
5. Yamamoto, N.; Kijima, H.; Nagamoto, H.; Kurokawa, D.; Takahashi, H.; Sano, H.; Itoi, E. Outcome of Bankart repair in contact versus non-contact athletes. *Orthop. Traumatol. Surg. Res.* **2015**, *101*, 415–419. [CrossRef] [PubMed]
6. Sonone, S.V.; Sasun, A.; Lanke, P.; Phansopkar, P. Outcome analysis of accelerated physiotherapy rehabilitation following arthroscopic repair of Bankart lesion and soft tissue reconstruction: A case report. *Med. Sci.* **2022**, *26*, ms250e2252. [CrossRef]
7. Almajed, Y.A.; Hall, A.C.; Gillingwater, T.H.; Alashkham, A. Anatomical, functional and biomechanical review of the glenoid labrum. *J. Anat.* **2022**, *240*, 761–771. [PubMed]
8. Nakagawa, S.; Iuchi, R.; Mae, T.; Mizuno, N.; Take, Y. Clinical outcome of arthroscopic Bankart repair combined with simultaneous capsular repair. *Am. J. Sports Med.* **2017**, *45*, 1289–1296. [CrossRef] [PubMed]
9. Gatti, C.J.; Maratt, J.D.; Palmer, M.L.; Hughes, R.E.; Carpenter, J.E. Development and validation of a finite element model of the superior glenoid labrum. *Ann. Biomed. Eng.* **2010**, *38*, 3766–3776. [CrossRef] [PubMed]

10. Maldonado, J.A.; Puentes, D.A.; Quintero, I.D.; González-Estrada, O.A.; Villegas, D.F. Image-based numerical analysis for isolated type II SLAP lesions in shoulder abduction and external rotation. *Diagnostics* **2023**, *13*, 1819. [CrossRef] [PubMed]
11. Suarez-Hernandez, M.D.L.L.; Urriolagoitia-Sosa, G.; Romero-Ángeles, B.; Carrasco-Hernández, F.; Martínez-Reyes, J.; Gallegos-Funes, F.J.; Velázquez-Lozada, E.; Correa-Corona, M.I.; German-Carcaño, J.M.; Urriolagoitia-Calderón, G.M. Numerical evaluation for SLAP type II tear in shoulder abduction applying the finite element method. *Front. Mech. Eng.* **2025**, *11*, 1505969. [CrossRef]
12. Yu, J.; Yin, Y.; Chen, W.; Mi, J. Long head of the biceps tendon plays a role in stress absorption and humeral head restriction during the late cocking and deceleration phases of overhead throwing: A finite element study. *J. Shoulder Elb. Surg.* **2025**, *34*, 699–709. [CrossRef]
13. Walia, P.; Miniaci, A.; Jones, M.H.; Fening, S.D. Theoretical model of the effect of combined glenohumeral bone defects on anterior shoulder instability: A finite element approach. *J. Orthop. Res.* **2013**, *31*, 601–607. [PubMed]
14. Feng, S.; Li, H.; Chen, Y.; Chen, J.; Ji, X.; Chen, S. Bankart repair with remplissage restores better shoulder stability than Bankart repair alone, and medial or two remplissage anchors increase stability but decrease range of motion: A finite element analysis. *Arthrosc. J. Arthrosc. Relat. Surg.* **2022**, *38*, 2972–2983. [CrossRef]
15. Hartzler, R.U.; Bui, C.N.; Jeong, W.K.; Akeda, M.; Peterson, A.; McGarry, M.; Lee, T.Q. Remplissage of an off-track Hill-Sachs lesion is necessary to restore biomechanical glenohumeral joint stability in a bipolar bone loss model. *Arthroscopy* **2016**, *32*, 2466–2476. [CrossRef] [PubMed]
16. Song, S.; Xie, Y.; Zhang, F.; Li, J.; Yang, J.; Xiong, W.; Fu, Y.; Li, J.; Zhu, Y.; Zhu, Y.; et al. Finite Element Analysis of Remplissage With Bankart Repair for Anterior Glenohumeral Instability: Reducing Anterior Humeral Head Displacement by Implanting Anchors in the Upper Region of Hill-Sachs Lesions. *Orthop. J. Sports Med.* **2026**, *14*, 23259671251399810. [CrossRef] [PubMed]
17. Zheng, M.; Zou, Z.; Bartolo, P.J.D.S.; Peach, C.; Ren, L. Finite element models of the human shoulder complex: A review of their clinical implications and modelling techniques. *Int. J. Numer. Methods Biomed. Eng.* **2017**, *33*, e02777. [CrossRef]
18. Xu, D.; Zhou, H.; Jie, T.; Zhou, Z.; Yuan, Y.; Jemni, M.; Quan, W.; Gao, Z.; Xiang, L.; Gusztav, F.; et al. Data-driven deep learning for predicting ligament fatigue failure risk mechanisms. *Int. J. Mech. Sci.* **2025**, *301*, 110519. [CrossRef]
19. Agathos, A.; Azariadis, P. 3D reconstruction of skeletal mesh models and human foot biomodel generation using semantic parametric-based deformation. *Int. J. Comput. Appl.* **2020**, *42*, 127–140.
20. Trejo-Enriquez, A.; Urriolagoitia-Sosa, G.; Romero-Ángeles, B.; García-Laguna, M.Á.; Guzmán-Baeza, M.; Martínez-Reyes, J.; Rojas-Castrejon, Y.Y.; Gallegos-Funes, F.J.; Patiño-Ortiz, J.; Urriolagoitia-Calderón, G.M. Numerical evaluation using the finite element method on frontal craniocervical impact directed at intervertebral disc wear. *Appl. Sci.* **2023**, *13*, 11989. [CrossRef]
21. Beristain-Lima, S.; Molina-Ballinas, A.; López-Suárez, O.; Benítez-García, H.A.; Romero-Ángeles, B.; Rodríguez-Cañizo, R.G. Análisis numérico de una prótesis de disco intervertebral. *Científica* **2013**, *17*, 55–65.
22. Maya-Anaya, D.; Urriolagoitia-Sosa, G.; Romero-Ángeles, B.; Martinez-Mondragon, M.; German-Carcaño, J.M.; Correa-Corona, M.I.; Trejo-Enriquez, A.; Sánchez-Cervantes, A.; Urriolagoitia-Luna, A.; Urriolagoitia-Calderón, G.M. Numerical analysis applying the finite element method by developing a complex three-dimensional biomodel of the biological tissues of the elbow joint using computerized axial tomography. *Appl. Sci.* **2023**, *13*, 8903. [CrossRef]
23. Serrato-Pedrosa, J.A.; Urriolagoitia-Sosa, G.; Romero-Ángeles, B.; Urriolagoitia-Calderón, G.M.; Cruz-López, S.; Urriolagoitia-Luna, A.; Carbajal-Luna, D.E.; Guereca-Ibarra, J.R.; Murillo-Aleman, G. Biomechanical evaluation of plantar pressure distribution towards a customized 3D orthotic device: A methodological case study through a finite element analysis approach. *Appl. Sci.* **2024**, *14*, 1650. [CrossRef]
24. Kadi, R.; Milants, A.; Shahabpour, M. Shoulder anatomy and normal variants. *J. Belg. Soc. Radiol.* **2017**, *101*, 3. [CrossRef] [PubMed]
25. Sun, C.; Zhong, B.; Pan, Z.; Du, D.; Min, X. Anatomical structure of the coracohumeral ligament and its effect on shoulder joint stability. *Folia Morphol.* **2017**, *76*, 720–729. [CrossRef]
26. Drury, N.J.; Ellis, B.J.; Weiss, J.A.; McMahon, P.J.; Debski, R.E. The impact of glenoid labrum thickness and modulus on labrum and glenohumeral capsule function. *J. Biomech. Eng.* **2010**, *132*, 121003. [CrossRef] [PubMed]
27. Tran, J.; Peng, P.W.H.; Agur, A.M.R. Anatomical study of the innervation of glenohumeral and acromioclavicular joint capsules: Implications for image-guided intervention. *Reg. Anesth. Pain Med.* **2019**, *44*, 452–458. [CrossRef]
28. Santos, R.B.M.; Prazeres, C.M.M.; Fittipaldi, R.M.; Monteiro, J.; Nogueira, T.C.L.; Santos, S.M. Bankart lesion repair: Biomechanical and anatomical analysis of Mason-Allen and simple sutures in a swine model. *Rev. Bras. DE Ortop.* **2018**, *53*, 454–459. [CrossRef]
29. Cho, Y. Volume of a tetrahedron in terms of dihedral angles and circumradius. *Appl. Math. Lett.* **2000**, *13*, 45–47. [CrossRef]
30. Weisstein, E.W. Regular Tetrahedron. MathWorld—A Wolfram Web Resource. Available online: https://mathworld.wolfram.com/RegularTetrahedron.html (accessed on 11 February 2026).
31. ANSYS, Inc. *ANSYS Meshing Training Manual: Appendix A—Mesh Quality Metrics*; ANSYS, Inc.: Canonsburg, PA, USA, 2009.
32. ANSYS, Inc. *Lecture 8—Mesh Quality, ANSYS Course Notes*; ANSYS, Inc.: Canonsburg, PA, USA, 2012.
33. Liu, J.; Zhang, Z.; Li, P.; Piao, C. Enhancing fixation stability in proximal humerus fractures: Screw orientation optimization in PHILOS plates through finite element analysis and biomechanical testing. *Sci. Rep.* **2024**, *14*, 27064. [CrossRef] [PubMed]

34. de la Luz Suarez-Hernandez, M.; Urriolagoitia-Sosa, G.; Guereca-Ibarra, J.R.; Ramirez-Sanchez, G.; Rojas-Castrejon, Y.Y.; Rodriguez-Granados, E.J.; Antonio Vargas-Bustos, J. Comparative Study of the Mesh Quality of the Soft Tissues of the Shoulder Joint: A Finite Element Analysis. In *Computer Vision Conference*; Springer Nature: Cham, Switzerland, 2026; pp. 273–285.
35. Hughes, T.J.R.; Liu, W.K. Nonlinear finite element analysis of shells; part I. Three-dimentional shells. *Comput. Methods Appl. Mech. Eng.* **1981**, *26*, 331–362. [CrossRef]
36. Hughes, T.J.R.; Liu, W.K. Nonlinear finite element analysis of shells-part II. Two-dimentional shells. *Comput. Methods Appl. Mech. Eng.* **1981**, *27*, 167–181. [CrossRef]
37. Zheng, M.; Qian, Z.; Zou, Z.; Peach, C.; Akrami, M.; Ren, L. Subject-specific finite element modelling of the human shoulder complex part 1; Model construction and quasi-static abduction simulation. *J. Bionic Eng.* **2020**, *17*, 1224–1238. [CrossRef]
38. Kim, M.S.; Lim, K.Y.; Lee, D.H.; Kovacevic, D.; Cho, N.Y. How does scapula motion change after reverse total shoulder arthroplasty?—A preliminary report. *Biomed. Cent. Musculoskelet. Disord.* **2012**, *13*, 210. [CrossRef]
39. Wu, G.; Van der Helm, F.C.; Veeger, H.D.; Makhsous, M.; Van Roy, P.; Anglin, C.; Nagels, J.; Karduna, A.R.; McQuade, K.; Wang, X.; et al. ISB recommendation on definitions of joint coordinate systems of various joints for the reporting of human joint motion—Part II: Shoulder, elbow, wrist and hand. *J. Biomech.* **2005**, *38*, 981–992. [CrossRef] [PubMed]
40. Gava, V.; Rosa, D.P.; Pereira, N.D.; Phadke, V.; Camargo, P.R. Ratio between 3D glenohumeral and scapulothoracic motions in individuals without shoulder pain. *J. Electromyogr. Kinesiol.* **2022**, *62*, 102623. [CrossRef] [PubMed]
41. Yano, Y.; Hamada, J.; Tamai, K.; Yoshizaki, K.; Sahara, R.; Fujiwara, T.; Nohara, Y. Different scapular kinematics in healthy subjects during arm elevation and lowering; Glenohumeral and scapulothoracic patterns. *J. Shoulder Elb. Surg.* **2010**, *19*, 209–215. [CrossRef]
42. Kunnil, M.; Yamarthi, D.; Kompally, S.K. Finite element analysis of elastomers using ANSYS. In Proceedings of the 2012 20th International Conference on Nuclear Engineering and the ASME 2012 Power Conference, Anaheim, CA, USA, 30 July–3 August 2012; Volume 44960, pp. 75–82.
43. Moskvichev, E.N.; Porokhin, A.V.; Shcherbakov, I.V. Numerical modeling of the strain of elastic rubber elements. *J. Phys. Conf. Ser.* **2017**, *919*, 012014. [CrossRef]
44. Johnson, J.E.; Caceres, A.P.; Anderson, D.D.; Patterson, B.M. Postimpingemnt instability following reverse shoulder arthroplasty: A parametric finite analysis. *Semin. Arthroplast. JSES* **2021**, *31*, 36–44. [CrossRef]
45. Jang, S.W.; Yoo, Y.S.; Lee, H.Y.; Kim, Y.S.; Srivastava, P.K.; Nair, A.V. Stress distribution in superior labral complex and rotator cuff during in vivo shoulder motion: A finite element analysis. *Arthrosc. J. Arthrosc. Relat. Surg.* **2015**, *31*, 2073–2081. [CrossRef]
46. Duprey, S.; Bruyere, K.; Verriest, J.P. Human shoulder response to side impacts: A finite element study. *Comput. Methods Biomech. Biomed. Eng.* **2007**, *10*, 361–370. [CrossRef]
47. Bodapati, V. Strain Analysis in Glenohumeral Capsule Through Finite Element Modelling. Doctoral Dissertation, University of Illinois at Urbana-Champaign, Champaign, IL, USA, 2019.
48. Jang, S.W.; Yoo, Y.S.; Kim, Y.S. A new method of contact stress measurement for analyzing internal impingement syndrome of the shoulder: Potentials and preliminary evaluation. *Appl. Sci.* **2020**, *10*, 4165. [CrossRef]
49. Dumont, G.D.; Russell, R.D.; Robertson, W.J. Anterior shoulder instability: A review of pathoanatomic, diagnosis and treatment. *Curr. Rev. Musculoskelet. Med.* **2011**, *4*, 200–207. [CrossRef] [PubMed]
50. Kaptan, A.Y.; Özer, M.; Alim, E.; Perçin, A.; Ayanoğlu, T.; Öztürk, B.Y.; Kanatli, U. The middle glenohumeral ligament: A classification based on arthroscopic evaluation. *J. Shoulder Elb. Surg.* **2022**, *31*, e83–e91. [CrossRef]
51. Klemt, C.; Nolte, D.; Grigoriadis, G.; Di Federico, E.; Reilly, P.; Bull, A.M. The contribution of the glenoid labrum to glenohumeral stability under physiological joint loading using finite element analysis. *Comput. Methods Biomech. Biomed. Eng.* **2017**, *20*, 1613–1622. [CrossRef]
52. Waterman, B.R.; Kilcoyne, G.; Parada, S.A.; Eichinger, J.K. Prevention and management of post-instability glenohumeral arthropathy. *World J. Orthop.* **2017**, *8*, 229–241. [CrossRef] [PubMed]
53. Coifman, I.; Brunner, U.H.; Scheibel, M. Dislocation arthropathy of the shoulder. *J. Clin. Med.* **2022**, *11*, 2019. [CrossRef] [PubMed]
54. Adams, C.R.; DeMartino, A.M.; Rego, G.; Denard, P.J.; Burkhart, S.S. The rotator cuff and the superior capsule: Why we need both. *Arthrosc. J. Arthrosc. Relat. Surg.* **2016**, *32*, 2628–2637. [CrossRef]

https://doi.org/10.3390/applmech7030061